

Study of Neutral Fe(III) Complexes of Pyridoxal-*N*-Substituted Thiosemicarbazone with Desolvation-Induced Spin-State Transformation above Room Temperature

Eddy W. Yemeli Tido,^{†‡} Gert O. R. Alberda van Ekenstein,[‡] Auke Meetsma,[‡] and Petra J. van Koningsbruggen^{*†‡}

Stratingh Institute for Chemistry and Zernike Institute for Advanced Materials, University of Groningen, Nijenborgh 4, 9747 AG Groningen, The Netherlands

Received August 29, 2007

The preparation and characterization of two new neutral ferric complexes with desolvation-induced discontinuous spin-state transformation above room temperature are reported. The compounds, [Fe(Hthpy)(thpy)]·CH₃OH·3H₂O (**1**) and [Fe(Hmthpy)(mthpy)]·2H₂O (**2**), are low-spin (LS) at room temperature and below, whereas their nonsolvated forms are high-spin (HS), exhibiting zero-field splitting. In these complexes, Hthpy, Hmthpy, and thpy, mthpy are the deprotonated forms of pyridoxal thiosemicarbazone and pyridoxal methylthiosemicarbazone, respectively; each is an O,N,S-tridentate ligand. The molecular structures have been determined at 100(1) K using single-crystal X-ray diffraction techniques and resulted in a triclinic system (space group $P\bar{1}$) and monoclinic unit cell (space group $P2_1/c$) for **1** and **2**, respectively. Structures were refined to the final error indices, where $R_F = 0.0560$ for **1** and $R_F = 0.0522$ for **2**. The chemical inequivalence of the ligands was clearly established, for the “extra” hydrogen atom on the monodeprotonated ligands (Hthpy, Hmthpy) was found to be bound to the nitrogen of the pyridine ring. The ligands are all of the thiol form; the doubly deprotonated chelates (thpy, mthpy) have C–S bond lengths slightly longer than those of the singly deprotonated forms. There is a three-dimensional network of hydrogen bonds in both compounds. The discontinuous spin-state transformation is accompanied with liberation of solvate molecules. This is evidenced also from DSC analysis. Heat capacity data for the LS and HS phases are tabulated at selected temperatures, the values of the enthalpy and entropy changes connected with the change of spin state were reckoned at $\Delta H = 12.5 \pm 0.3 \text{ kJ mol}^{-1}$ and $\Delta S = 33.3 \pm 0.8 \text{ J mol}^{-1} \text{ K}^{-1}$, respectively, for **1** and $\Delta H = 6.5 \pm 0.3 \text{ kJ mol}^{-1}$ and $\Delta S = 17.6 \pm 0.8 \text{ J mol}^{-1} \text{ K}^{-1}$, respectively, for **2**.

Introduction

Octahedral transition metal complexes with the configuration $3d^4$, $3d^5$, $3d^6$, and $3d^7$ are expected to exhibit spin-crossover behavior when the energy difference between the low-spin (LS) and high-spin (HS) states is in the range of kT .^{1–4} Since this requirement is very restrictive, only a few classes of transition metal complexes featuring low-spin ↔

high-spin equilibria are well-documented. For instance, the monomeric iron(III) complexes with tridentate *O,N,S*-thiosemicarbazone ligands were the first representatives of a large class of chelates that can exhibit the $S = 5/2 \leftrightarrow S = 1/2$ spin transition at attainable temperatures.⁵ Following the pioneering synthesis and characterization of the neutral complex of this family of Schiff base type ligands,^{6,7} Timken et al.⁸ determined the crystal structure of [Cr(Hthpu)(thpu)]·H₂O

* To whom correspondence should be addressed. Phone: +31 (0)-50-363 4363. Fax: +31 (0)-50-363 4315. E-mail: P.J.van.Koningsbruggen@rug.nl.

[†] Stratingh Institute for Chemistry.

[‡] Zernike Institute for Advanced Materials.

- (1) Gütlich, P.; Hauser, A.; Spiering, H. *Angew. Chem.* **1994**, *106*, 2109; *Angew. Chem., Int. Ed. Engl.* **1994**, *33*, 2024.
- (2) Gütlich, P. *Struct. Bonding (Berlin)* **1981**, *44*, 83.
- (3) Kahn, O. *Molecular Magnetism*; WILEY-VCH: New York 1993; Chapter 4, p 53 ff.
- (4) Goodwin, H. A. *Coord. Chem. Rev.* **1976**, *18*, 293.

- (5) (a) Zelentsov, V. V. *Russ. J. Coord. Chem. (Engl. Transl.)* **2003**, *29*, 425. (b) Zelentsov, V. V. *Sov. Sci. Rev. B. Chem.* **1987**, *10*, 485. (c) Kogan, V. A.; Zelentsov, V. V.; Larin, G. M.; Lukov, V. V. *Kompleksy Perekhodnykh Metallov s Gidrazonami: Fiziko-khimicheskie Svoistva i Stroenie (Complexes of Transition Metals with Hydrazones: Physicochemical Properties and Structure)*; Nauka: Moscow, 1990; p 85.
- (6) Ablov, A. V.; Gerbeleu, N. V. *Russ. J. Inorg. Chem.* **1965**, *10*, 33.
- (7) Ablov, A. V.; Gerbeleu, N. V. *Russ. J. Inorg. Chem.* **1970**, *15*, 952.
- (8) Timken, M. D.; Wilson, S. R.; Hendrickson, D. N. *Inorg. Chem.* **1985**, *24*, 3450.

(where Hthpu and thpu are the singly and doubly deprotonated forms of pyruvic acid thiosemicarbazone) and showed that the room-temperature X-ray powder diffraction pattern is isostructural to that of $[\text{Fe}(\text{Hthpu})(\text{thpu})]\cdot\text{H}_2\text{O}$. The iron type of its nonhydrated form showed an abrupt transition with associated thermal hysteresis ($T_{1/2}^{\downarrow} = 225 \text{ K}$ and $T_{1/2}^{\uparrow} = 235 \text{ K}$). Further study⁹ showed photoswitchable behavior at low temperature ($T = 5 \text{ K}$), albeit with low photoefficiency (about 2%). It is worth noting, however, that its powder diffraction diagram was not isostructural to either of the hydrated materials, due to the significant role that water molecules play in forming the extensive hydrogen-bonding network found in the chromium structure. Afterward, Belicchi et al.¹⁰ reported the crystal structure of $[\text{Co}^{\text{III}}(\text{HL})\text{L}]\cdot 4.5\text{H}_2\text{O}$, where HL and L are the mono- and dianionic form of pyridoxal thiosemicarbazone. Despite the good structural determination of the molecular compound, its synthesis involves some intriguing features: first, because the starting material was a Co^{II} salt and, second, the pH range referred to did not correspond with the literature, in view of the deprotonation sequence, on pyridoxal-N-substituted thiosemicarbazone.^{11–13}

In addition, literature presents metal complexes of various terdentate X-semicarbazones ($\text{X} = \text{S}, \text{Se}$),^{14–20} with the ligand attached to the central metal ion in two different deprotonated forms, but the structural features of the complexes remain unclear because they have not been made explicit. In any case, the reason put forward to explain the unusual nature of the inequivalency of the ligands is the different tautomeric forms one can find the chelate in in solution, but the pH at which those compounds are formed is often overlooked. With pyridoxal-N-substituted thiosemicarbazone, the situation is more or less different because the inequivalent ligands are all of the thiol form. In this work, we described for the first time the synthesis and structural characterization of two new neutral iron(III) complexes of pyridoxal-N-substituted thiosemicarbazone, bringing about the pH range of formation of these complexes. Moreover, the low- and high-temperature magnetic behavior is revealed even for the nonhydrated complexes. The data on the heat capacities of compounds are given. The enthalpy and entropy changes from low- to high-spin are calculated and compared with published values.

- (9) Hayami, S.; Hashiguchi, K.; Inoue, K.; Maeda, Y. *J. Nucl. Radiochem. Sci.* **2004**, 5, N1.
- (10) Belicchi Ferrari, M.; Fava, G. G.; Lanfranchi, M.; Pelizzi, C.; Tarasconi, P. *J. Chem. Soc., Dalton Trans.* **1991**, 1951.
- (11) Leovac, V. M.; Jevtovic, V. S.; Jovanovic, L. S.; Bogdanovic, G. A. *J. Serb. Chem. Soc.* **2005**, 70, 393.
- (12) Bendito, D. P.; Valcárcel, M. *Afinidad* **1980**, 37, 123.
- (13) Ballesteros, L.; Bendito, D. P. *Mikrochim. Acta* **1986**, I, 123.
- (14) Ablov, A. V.; Goldanskii, V. I.; Turta, K. I.; Stukan, R. A.; Zelentsov, V. V.; Ivanov, E. V.; Gerbeleu, N. V. *Dokl. Phys. Chem. (Engl. Transl.)* **1971**, 196, 134.
- (15) Ablov, A. V.; Gerbeleu, N. V. *Russ. J. Inorg. Chem.* **1964**, 9, 1260.
- (16) Ablov, A. V.; Bologna, O. A. *Russ. J. Inorg. Chem.* **1977**, 22, 127.
- (17) Bologna, O. A.; Belichuk, N. I.; Ablov, A. V. *Russ. J. Inorg. Chem.* **1978**, 23, 1036.
- (18) Zelentsov, V. V.; Larin, G. M.; Ivanov, E. V.; Gerbeleu, N. V.; Ablov, A. G. *Theor. Exp. Chem. (Engl. Transl.)* **1971**, 7, 648.
- (19) Belicchi Ferrari, M.; Fava Gasparri, G.; Pelosi, G.; Rodriguez-Argüelles, M. C.; Tarasconi, P. *J. Chem. Soc., Dalton Trans.* **1995**, 3035.
- (20) Jovanovic, L. S.; Jevtovic, V. S.; Leovac, V. M.; Bjelica, L. J. *J. Serb. Chem. Soc.* **2005**, 70, 187.

Experimental Section

Reagents and Materials. Pyridoxal hydrochloride (99%) and iron(III) *p*-toluenesulfonate $[\text{Fe}(\text{CH}_3\text{C}_6\text{H}_4\text{SO}_3)_3\cdot 6\text{H}_2\text{O}]$ were purchased from Aldrich, whereas thiosemicarbazide (99%), 4-methyl-3-thiosemicarbazide (97%), and iron(III) nitrate nanohydrate $[\text{Fe}(\text{NO}_3)_3\cdot 9\text{H}_2\text{O}]$ were purchased from Acros. All chemicals were used without further purification.

Syntheses. Pyridoxal Thiosemicarbazone Hydrochloride ($\text{H}_2\text{thpy}\cdot\text{HCl}$). $\text{H}_2\text{thpy}\cdot\text{HCl}$ was prepared according to a procedure described in literature.²¹ Yield: 12.83 g (46.40 mmol, 94.5%). Mp: 212 °C. Anal. Calcd for $\text{C}_9\text{H}_{13}\text{N}_4\text{O}_2\text{S}\cdot\text{HCl}$: C, 39.06; H, 4.73; N, 20.25; S, 11.58. Found: C, 39.08; H, 4.74; N, 20.07; S, 11.60. $\text{H}_2\text{thpy}\cdot\text{HCl}$ is soluble in water and ethanol, but scarcely dissolves in acetone, chloroform, and methanol, even at elevated temperatures. ¹H NMR (300 MHz, DMSO-*d*₆) δ (ppm): 11.60 (s, br, 1H, NH-3), 9.65 (s, br, 1H, OH py), 8.56 (s, 1H, HC=N), 8.33 and 8.10 (s, br, 2H, NH₂), 7.98 (s, 1H, py), 5.26 (t, 1H, OH), 4.57 (d, 2H, py CH₂O), 2.39 (s, 3H, CH₃ py). MS (ionization mode: EI+) *m/z* (%): 240 (71), 165 (100), 150 (41), 119 (11), 77 (23), 60 (17). IR (cm⁻¹, KBr): 3293.6 (m), 3153.9 (br), 3042.1 (w), 2760.8 (br), 1640.8 (vs), 1571.5 (s), 1474.5 (m), 1358.9 (s), 1256.2 (m), 1185.5 (vs), 1063.5 (s), 1017.3 (vs), 910.0 (m), 878.5 (m), 780.9 (m), 756.5 (m), 646.1 (s), 565.8 (w).

Pyridoxal-4-methylthiosemicarbazone Hydrochloride ($\text{H}_2\text{mthpy}\cdot\text{HCl}$). $\text{H}_2\text{mthpy}\cdot\text{HCl}$ was prepared as previously described.²¹ Yield: 9.0 g (30.98 mmol, 63%). Mp: 228 °C. Anal. Calcd for $\text{C}_{10}\text{H}_{14}\text{N}_4\text{O}_2\text{S}\cdot\text{HCl}$: C, 41.31; H, 5.20; N, 19.27; S, 11.03. Found: C, 41.30; H, 5.18; N, 19.10; S, 11.11. $\text{H}_2\text{mthpy}\cdot\text{HCl}$ is soluble in water and ethanol, but scarcely dissolves in acetone, chloroform, and methanol, even at elevated temperatures. ¹H NMR (300 MHz, DMSO-*d*₆) δ (ppm): 11.40 (s, br, 1H, OH py), 9.93 (s, br, 1H, NH-2), 8.59 (m, 2H, py CHN + NH-4), 7.93 (s, 1H, py), 5.29 (t, 1H, OH), 4.56 (d, 2H, py CH₂O), 2.99 (d, 3H, CH₃N), 2.42 (s, 3H, CH₃ py). MS (ionization mode: EI+) *m/z* (%): 254 (98), 165 (100), 150 (27), 116 (7), 74 (31), 57 (39). IR (cm⁻¹, KBr): 3197.9 (br), 2963.1 (w), 2921.4 (w), 2850.8 (w), 1615.2 (m), 1558.0 (vs), 1471.6 (m), 1396.2 (m), 1305.9 (vs), 1259.7 (m), 1236.9 (m), 1197.7 (s), 1043.6 (s), 1000.2 (vs), 859.3 (v), 770.0 (s), 948.2 (w), 859.3 (m), 770.3 (m), 667.6 (s), 589.2(s).

$[\text{Fe}(\text{Hthpy})(\text{thpy})]\cdot\text{CH}_3\text{OH}\cdot 3\text{H}_2\text{O}$. About 20 mL of concentrated ammonia was added to a mixture of pyridoxalthiosemicarbazone·HCl (0.553 g, 2 mmol) in 20 mL of water and $\text{Fe}(\text{CH}_3\text{C}_6\text{H}_4\text{SO}_3)_3\cdot 6\text{H}_2\text{O}$ (0.678 g, 1 mmol) in 20 mL of methanol with constant stirring. The resulting dark green solution was stirred and heated mildly up to 40 °C for about 15 min, before approximately 2 g of NH_4Cl salt was added. The final solution was stirred for 10 min and allowed to stand at room temperature for 5 days. The dark green microcrystals were isolated by filtration, washed with methanol and diethyl ether, and dried in a well-ventilated space for 24 h. Yield: 0.43 g (0.694 mmol, 68.8%). Mp: >280 °C. Anal. Calcd for $\text{C}_{19}\text{H}_{31}\text{N}_8\text{O}_8\text{S}_2\text{Fe}$: C, 36.84; H, 5.04; N, 18.09; S, 10.35. Found: C, 35.58; H, 4.80; N, 18.02; S, 10.23. The complex is soluble in concentrated acidic and basic solutions. IR (cm⁻¹, KBr): 3407.4 (br), 3310.9 (w), 1623.6 (vs), 1460.3 (vs), 1369.6 (s), 1316.3 (s), 1261.0 (m), 1210.2 (m), 1152.9 (m), 1011.5 (s), 907.9 (w), 759.4 (m), 612.2 (m), 565.2 (w).

$[\text{Fe}(\text{Hmthpy})(\text{mthpy})]\cdot 2\text{H}_2\text{O}$. A solution of $\text{Fe}(\text{NO}_3)_3\cdot 9\text{H}_2\text{O}$ (0.404 g, 1 mmol) in 15 mL of water was added dropwise to a mixture of concentrated ammonia (20 mL) and pyridoxal-4-methylthiosemicarbazone·HCl (0.582 g, 2 mmol) in 20 mL of water

- (21) Yemeli Tido, E. W.; Vertelman, E. J. M.; Meetsma, A.; van Koningsbruggen, P. J. *Inorg. Chim. Acta* **2007**, 360, 3896.

on constant stirring. The resulting dark green solution was stirred and heated mildly up to 40 °C for about 10 min, whereafter approximately 2 g of NH₄Cl salt was added. The final solution was stirred for 10 min and allowed to stand at room temperature for 3 days. The dark green microcrystals were isolated by filtration, washed with water and diethyl ether, and dried in a well-ventilated space for 24 h. Yield: 0.323 g (0.541 mmol, 54.1%). Mp: >280 °C. Anal. Calcd for C₂₀H₂₉N₈O₆S₂Fe: C, 40.21; H, 4.89; N, 18.75; S, 10.73. Found: C, 39.30; H, 4.99; N, 18.42; S, 10.57. The complex is soluble in concentrated acidic and basic media. IR (cm⁻¹, KBr): 1508.5 (vs), 1392.8 (m), 1363.8 (s), 1304.0 (s), 1252.0 (w), 1206.9 (m), 1169.7 (m), 1093.8 (m), 1017.9 (s).

Physical Measurements. The pH of the solution was measured using a calibrated glass electrode on a Microprocessor pH 213 pH-meter of HANNA instruments. In all measurements the temperature ranged from 18.0 ± 0.1 to 22.0 ± 0.1 °C. Infrared spectra were recorded on KBr pellets with an Interspec 200-X FT-IR spectrometer in the range between 4000 and 400 cm⁻¹ with a resolution of 1 cm⁻¹ (w, weak; br, broad; m, medium; s, strong; vs, very strong). Routine EI+ spectra were measured with the MS route JMS-600H sector mass spectrometer (JEOL). ¹H NMR spectra were recorded in DMSO-*d*₆ with a Varian VXR 300 spectrometer with TMS as standard (s, singlet; d, doublet; t, triplet; m, multiplet; s, br, singlet, broad). Elemental analysis was carried out at the Microanalytical Department of the University of Groningen, using the Euro EA Elemental Analyzer from EuroVector Instrument and Software Co. The magnetic measurements were performed on a Quantum Design magnetometer with a superconducting quantum interface device. The sample was prepared by putting an exact weight of the compound between two pieces of cotton wool in a gelcap. The magnetic field was kept constant at 0.1 T while the temperature was raised from 5 to 300 K during low-temperature measurements and from 200 to 375 K during high-temperature measurements. The collected raw data were corrected for molecular diamagnetism.

Thermal Analysis. The heat flow was recorded using a DSC 2920 MDSC of TA-Instruments with 10 °C/min scan rate in the temperature range of 20–180 °C.

Heat capacity measurements were performed with a Q1000 MDSC of TA-Instruments in the modulated mode. The heating rate was 2 °C/min, amplitude 0.5 °C, and period 60 s. The heat capacity constant was calibrated using sapphire, and details of the thermodynamic calibration are given elsewhere.²² For heat capacity determination, samples were equilibrated at -40 °C, heated to 40 °C (LS) for the solvent-containing compounds and to 150 °C (HS) for the dry compounds.

Thermogravimetric measurements were carried out using a Perkin-Elmer TGA7 apparatus in the temperature range 25–250 °C under inert atmosphere (N₂) with 5 °C/min heating rate.

Data Processing. Recorded heat capacities were processed by a well-known procedure described in the literature.^{23,24} Every substance, regardless of whether it has unpaired spins or not, exhibits a lattice heat capacity. Therefore, the lattice heat capacity has to be evaluated in order to subtract it from the total to find the magnetic contribution. Because many of the magnetic contributions have a T^{-2} dependence for the specific heat in the high-temperature limit and the lattice specific heat follows the T^3 law in the measured temperature region, we assumed that the total experimental heat capacity in such a situation should obey the relationship $C_{p,exp} =$

$aT^3 + bT^{-2}$. By asserting that the aforementioned function holds true, we plotted $C_{p,exp}T^2$ vs T^5 and show the applicability of the procedure; i.e., we obtained a linear curve within the measured temperature region (Figure 11) and afterward we evaluated the a and b constants. However, since the spin state change is accompanied by the liberation of solvate molecules, data points below the initial peak temperature were used to determine the constants a_{LS} (b_{LS}) and data points above the final peak temperature to fit the constants a_{HS} (b_{HS}). Extrapolation to lower temperatures then allows an empirical evaluation of the lattice contribution in each case. The magnetic contribution to the heat capacity was estimated as shown from the following equations:

$$C_{p,mag} = C_{p,exp} - a_{LS}T^3 \quad \text{for } T < T_p \quad (1)$$

$$C'_{p,mag} = C'_{p,exp} - a_{HS}T^3 \quad \text{for } T > T_p \quad (2)$$

where T_p is the peak maximum temperature.

Afterward, the enthalpy related to the transition was evaluated numerically in two steps:

$$\Delta H = \int_{T_{HS}}^{T_{HS}'} C'_{p,mag} dT - \int_{T_{LS}}^{T_{LS}'} C_{p,mag} dT \quad (3)$$

The difference between the HS and the LS function is the excess enthalpy.

Finally, the entropy was easily calculated from the following quotient:

$$\Delta S = \frac{\Delta H}{T_c} \quad (4)$$

where T_c is the critical temperature or spin transition temperature.

X-ray Crystallography. Green, platelet-shaped crystals with the dimensions of 0.27 × 0.23 × 0.07 mm for **1** and of 0.35 × 0.11 × 0.03 mm for **2** were mounted on top of a glass fiber and aligned on a Bruker SMART APEX CCD diffractometer (platform with full three-circle goniometer). The diffractometer was equipped with a 4 K CCD detector set 60.0 mm from the crystal. The crystal was cooled to 100(1) K using the Bruker KRYOFLEX low-temperature device. Intensity measurements were performed using graphite-monochromated Mo K α radiation from a sealed ceramic diffraction tube (SIEMENS). Generator settings were 50 kV/40 mA. SMART²⁵ was used for preliminary determination of the unit cell constants and data collection control. The intensities of reflections of a hemisphere were collected by a combination of three sets of exposures (frames). Each set had a different ϕ angle for the crystal and each exposure covered a range of 0.3° in ω . A total of 1800 frames was collected with an exposure time of 20.0 s per frame and an overall data collection time of 13.5 h for **1** and 30.0 s per frame and an overall data collection time of 18.1 h for **2**. Data integration and global cell refinement was performed with the program SAINT.²⁵ The final unit cell was obtained from the xyz centroids of 2956 reflections for **1** and of 7811 reflections for **2** after integration. Intensity data were corrected for Lorentz and polarization effects, scale variation, and for decay and absorption: a multiscan absorption correction was applied on the basis of the intensities of symmetry-related reflections measured at different angular settings (SADABS),²⁶ and reduced to F_o^2 . The program suite SAINTPLUS was used for space group determination (XPREP).²⁵

(22) Höhne, G. W. H.; Hemminger, W. F.; Flammersheim, H. J. *Differential Scanning Calorimetry*; 2nd ed.; Springer: Berlin, 2003; p 298.

(23) Carlin, R. L. *Magnetochemistry*; Springer: Berlin, 1986; p 328.

(24) Carlin, R. L.; van Duynveldt, A. J. *Magnetic Properties of Transition Metal Compounds*; Springer: New York, 1977; p 264.

(25) SMART, SAINTPLUS and XPREP, Area Detector Control and integration Software, Smart Apex Software Reference Manuals; Bruker Analytical X-ray Instruments Inc.: Madison, WI, 2000.

(26) Sheldrick, G. M. *SADABS Version 2.03, Multi-Scan Absorption Correction Program*; University of Göttingen: Göttingen, Germany, 2001.

The unit cells^{27,28} were identified as triclinic, space group $P\bar{1}$ for **1** and as monoclinic, space group $P2_1/c$ for **2**. Examination of the final atomic coordinates of the structure did not yield extra crystallographic or metric symmetry elements.^{29,30}

The structures were solved by direct methods using the program SIR2002³¹ for **1**; Patterson methods and extension of the model was accomplished by direct methods applied to difference structure factors using the program DIRDIF³² for **2**. The positional and anisotropic displacement parameters for the non-hydrogen atoms were refined. A subsequent difference Fourier synthesis resulted in the location of all the hydrogen atoms, with coordinates, and isotropic displacement parameters were refined. For **1**, refinement was frustrated by a disorder problem: from the solution, it was clear that the atom positions of the solvate molecules were highly disordered, suggesting dynamic disorder (dynamic means that the smeared electron density is due to fluctuations of the atomic positions within each unit cell as a consequence of translational and rotational disorder); the disorder is compensated by the larger the displacement parameters. The electron density for methanol solvate molecule has been described by two sites, each with an site occupancy factor (sof) of 0.5.

Final refinement on F^2 carried out by full-matrix least-squares techniques converged at $wR(F^2) = 0.1424$ for 4874 reflections and $R(F) = 0.0560$ for 3702 reflections with $F_o \geq 4.0\sigma(F_o)$ and 469 parameters with nine restraints for **1** and $wR(F^2) = 0.1194$ for 4599 reflections and $R(F) = 0.0522$ for 3454 reflections with $F_o \geq 4.0\sigma(F_o)$ and 450 parameters for **2**.

A final difference Fourier map revealed features within the range -0.9 to $+1.6(1)$ e/Å³ located near the “dynamic” solvate molecules for complex **1** and was featureless for **2**.

The positional and anisotropic displacement parameters for the non-hydrogen atoms and isotropic displacement parameters for hydrogen atoms were refined on F^2 with full-matrix least-squares procedures minimizing the function $Q = \sum_h [w(|(F_o)^2 - k(F_c^2)|)]^2$, where $w = 1/[\sigma^2(F_o^2) + (aP)^2 + bP]$, $P = [\max(F_o^2, 0) + 2F_c^2]/3$, and F_o and F_c are the observed and calculated structure factor amplitudes, respectively; ultimately the suggested a ($=0.0588$) and b ($=3.20$) for **1** and a ($=0.0524$) and b ($=2.4341$) for **2** were used in the final refinement.

Crystal data and numerical details on data collection and refinement are given in Table 1. Neutral atom scattering factors and anomalous dispersion corrections were taken from *International Tables for Crystallography*.³³ All refinement calculations and graphics were performed on a HP XW6200 (Intel XEON 3.2 GHz)/Debian–Linux computer at the University of Groningen with the program packages SHELXL³⁴ (least-square refinements), a locally modified version of the program PLUTO³⁵ (preparation of illustrations) and PLATON³⁶ package (checking the final results for missed symmetry with the MISSYM option, solvent accessible voids with

Table 1. Crystal Data and Refinement Details of the Structure Determination of [Fe(Hthpy)(thpy)]·CH₃OH·3H₂O (**1**) and [Fe(Hmthpy)(mthpy)]·2H₂O (**2**)

	1	2
formula	C ₁₉ H ₃₁ FeN ₈ O ₈ S ₂	C ₂₀ H ₂₉ FeN ₈ O ₆ S ₂
formula weight (g mol ⁻¹)	619.48	597.48
crystal system	triclinic	monoclinic
space group	$P\bar{1}$	$P2_1/c$
crystal color	dark green	dark green
crystal description	platelet-shaped	platelet-shaped
crystal dimensions (mm)	0.27 × 0.23 × 0.07	0.35 × 0.11 × 0.03
unit cell dimensions		
<i>a</i> (Å)	10.701(2)	11.599(1)
<i>b</i> (Å)	10.846(2)	24.273(2)
<i>c</i> (Å)	11.910(2)	9.0649(9)
α (deg)	83.347(3)	
β (deg)	83.896(3)	107.589(2)
γ (deg)	68.914(3)	
volume (Å ³)	1278.0(4)	2432.8(4)
<i>Z</i>	2	4
<i>c/a</i>	1.1130	0.7815
D_{calc} (g cm ⁻³)	1.610	1.631
temperature (K)	100(1)	100(1)
radiation (Å)	0.71073	0.71073
μ (Mo K α) (cm ⁻¹)	8.15	8.47
$F(000)$	646	1224
number of unique data	4874	4599
number of data with $[F_o \geq 4.0\sigma(F_o)]$	3702	3454
$R(F)$, ^a $wR(F^2)$ ^b	0.0560, 0.1424	0.0522, 0.1194

^a $R(F) = \sum(|F_o| - |F_c|)/\sum|F_o|$ for $F_o > 4.0\sigma(F_o)$. ^b $wR(F^2) = [\sum[w(F_o^2 - F_c^2)^2]/\sum[w(F_o^2)^2]]^{1/2}$ with $w = 1/[\sigma^2(F_o^2) + (aP)^2 + bP]$ and $P = [\max(F_o^2, 0) + 2F_c^2]/3$ and weighting scheme $a = 0.0588$, $b = 3.20$ for **1** and $a = 0.0524$, $b = 2.4341$ for **2**.

the SOLV option, calculation of geometric data and the ORTEP³⁶ illustrations).

Supplementary crystallographic data for this paper are available from the IUCr electronic archives (Reference: CCDC 658152 for **2** and CCDC 658153 for **1**, as a CIF file). These data can be obtained free of charge via www.ccdc.cam.ac.uk/conts/retrieving.html (or from the Cambridge Crystallographic Data Centre, 12 Union Road, Cambridge CB2 1EZ, UK; fax (+44) 1223–336-033; or e-mail: deposit@ccdc.cam.ac.uk).

Results and Discussion

Influence of pH on the Synthesis. Many chemical transformations are sensitive to the presence of protons. Therefore, knowledge of the pH value, especially of the complex solution, is important in order to decide about its possible application. Because pH is dependent on activity, a property that cannot be measured easily or predicted theoretically, it is difficult to determine an accurate value for the pH of a solution. However, we carried out a pH study by recording day by day the pH of the complex solution until microcrystals were obtained. For this purpose H₂thpy·HCl was dissolved in an ammonia/water (1/1) mixture, and a methanolic solution of Fe(CH₃C₆H₄SO₃)₃·6H₂O was subsequently added to this. On the other hand, H₂mthpy·HCl was dissolved in an ammonia/water (1/1) mixture to which an aqueous solution of Fe(NO₃)₃·9H₂O was added. Testing revealed that the optimal base to be used was concentrated ammonia, even though experiments have revealed that

- (27) Spek, A. L. *J. Appl. Crystallogr.* **1988**, *21*, 578.
 (28) Duisenberg, A. J. M. *J. Appl. Crystallogr.* **1992**, *25*, 92.
 (29) Le Page, Y. *J. Appl. Crystallogr.* **1987**, *20*, 264.
 (30) Le Page, Y. *J. Appl. Crystallogr.* **1988**, *21*, 983.
 (31) SIR2002: Burla, M. C.; Camalli, M.; Carrozzini, B.; Cascarano, G. L.; Giacovazzo, C.; Polidori, G.; Spagna, R. *J. Appl. Crystallogr.* **2003**, *36*, 1103.
 (32) Beurskens, P. T.; Beurskens, G.; de Gelder, R.; García-Granda, S.; Gould, R. O.; Israël, R.; Smits, J. M. M. *The DIRDIF-99 program system*; Crystallography Laboratory, University of Nijmegen: Nijmegen, The Netherlands, 1999.
 (33) Wilson, A. J. C., Ed.; *International Tables for Crystallography*; Kluwer Academic Publishers: Dordrecht, The Netherlands 1992; Vol. C.
 (34) Sheldrick, G. M. *SHELXL-97, Program for the Refinement of Crystal Structures*; University of Göttingen: Göttingen, Germany, 1997.
 (35) Meetsma, A. *PLUTO, Molecular Graphics Program, Version of March 2006*; University of Groningen: Groningen, The Netherlands, 2006.

- (36) (a) Spek, A. L. *PLATON, Program for the Automated Analysis of Molecular Geometry (A Multipurpose Crystallographic Tool)*, Version of February 2006; University of Utrecht: Utrecht, The Netherlands 2006. (b) Spek, A. L. *J. Appl. Crystallogr.* **2003**, *36*, 7.

triethylamine could also be used, but in that instance it takes several weeks to obtain crystals. On the other hand, it was found that stronger bases (NaOH, KOH) were not suitable for this purpose, since no crystals were grown from such solutions. The pH range was defined as 9.0–11.5, in most cases, and crystal growth suitable for X-ray purpose came from solutions whose pH values lay between 10.40 and 10.70; otherwise, they are microcrystalline powders. The deprotonation sequence and pK_a constants of the ligands are known from previous studies.^{11–13} An addition of iron(III) salts influence predominantly the pH of the basic solution, but not to such an extent that it switches to a neutral or an acidic pH range. In the present study, the ligand binds to the metal ion in two inequivalent thiol forms, the mono-deprotonated form, which is known to have a pK_a equal to 7.9, and the di-deprotonated form, which is obtained from $pK_a \geq 11.2$. The complex solution can therefore be regarded as a nonclassical buffer solution due to the fact that it was not possible to go beyond the previously defined pH interval by subsequently adding the base or increasing its concentration. As it is known already from pyruvic acid X-semicarbazone and salicylaldehyde X-semicarbazone ($X = S, Se$),^{6,7,19,37,38} this neutral-type of compound is obtained by simply reacting metal salts and the ligands all dissolved in methanol, ethanol, or a mixture of each with water. Adding a base (soft or strong) leads in general to the anionic form of the complex,^{20,39,40} i.e., the ligand is attached to the metal ion of its doubly deprotonated form. Contrary to this expectation, it was not possible to obtain the complex with the ligand being twice deprotonated with pyridoxal-*N*-substituted thiosemicarbazone hydrochloride, because of the strong stability of the intermediate compound so formed. Accordingly, the cationic compound could not also be prepared, and an attempt generally leads to the decomposition of the material when using different strategies. In all, when the intermediate compound is formed in neutral or weakly acidic media, subsequent deprotonation is possible, whereas, if the medium is basic, further deprotonation will lead to unsuccessful results.

Molecular Structures Description. A perspective view of the molecular structure of the compounds is illustrated by the ORTEP³⁶ drawings in Figures 1 and 2. The packing of the molecules is presented in the respective unit cells and is displayed in Figures 3 and 4. Relevant information on bond lengths and angles is given in Table 2.

Compound **1** crystallizes in the triclinic space group $P\bar{1}$ with $Z = 2$. The asymmetric unit consists of one formula unit with no atom setting at a special position. The triclinic system contains two iron complexes, two highly disordered methanol solvate molecules, and six water solvate molecules. In contrast, compound **2** crystallizes in the monoclinic space

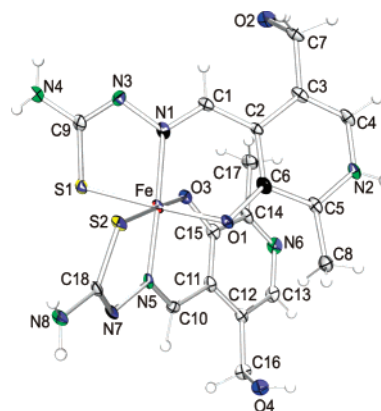


Figure 1. A perspective view (ORTEP drawing) of $[Fe(Hthpy)(thpy)] \cdot CH_3OH \cdot 3H_2O$ molecule with atom labeling. Non-hydrogen atoms are represented by thermal ellipsoids with 50% probability level.

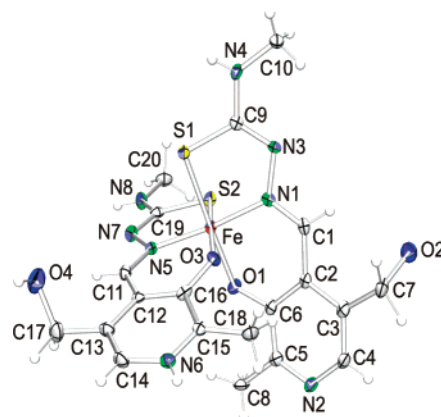


Figure 2. A perspective view (ORTEP drawing) of $[Fe(Hmthpy)(mthpy)] \cdot 2H_2O$ molecule with atom labeling. Non-hydrogen atoms are represented by thermal ellipsoids with 50% probability level.

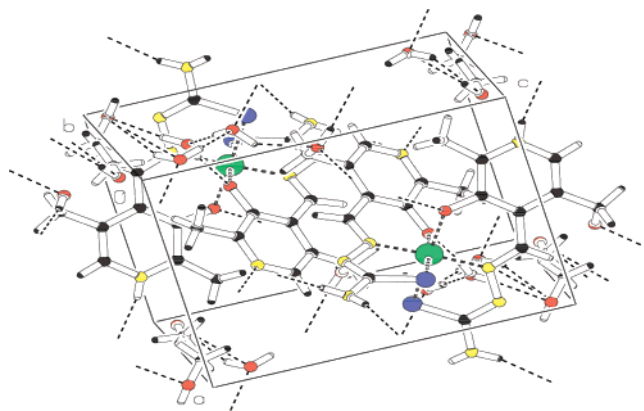


Figure 3. Packing arrangement of $[Fe(Hthpy)(thpy)] \cdot CH_3OH \cdot 3H_2O$ displayed in the unit cell.

group $P2_1/c$ with $Z = 4$. Its asymmetric unit consists of one formula unit without an atom at a special position. The unit cell contains four iron complexes and eight water molecules. The moieties of **1** and of **2** are linked by hydrogen bonds forming an infinite three-dimensional network along the base vectors.

In both compounds, the Fe(III) atom is coordinated by two inequivalent tridentate O,N,S-ligands, with the formation of a distorted $FeS_2N_2O_2$ octahedron. The donor atoms are located in mutually normal planes, the S and O atoms being

(37) Negryatse, N. Y.; Ablov, A. V.; Gerbeleu, N. V. *Russ. J. Inorg. Chem.* **1972**, *17*, 65.

(38) Ablov, A. V.; Gerbeleu, N. V.; Romanov, A. M. *Russ. J. Inorg. Chem.* **1968**, *13*, 1558.

(39) Zelentsov, V. V.; Yablokov, Y. V.; Jablokow, M. A. A.; Krupskaya, A.; Mrozinski, J.; Ulanov, V. A. *Chem. Phys.* **2004**, *301*, 15.

(40) Floquet, S.; Boillot, M.-L.; Rivière, E.; Varret, F.; Boukheddaden, K.; Morineau, D.; Négrier, P. *New J. Chem.* **2003**, *27*, 341.

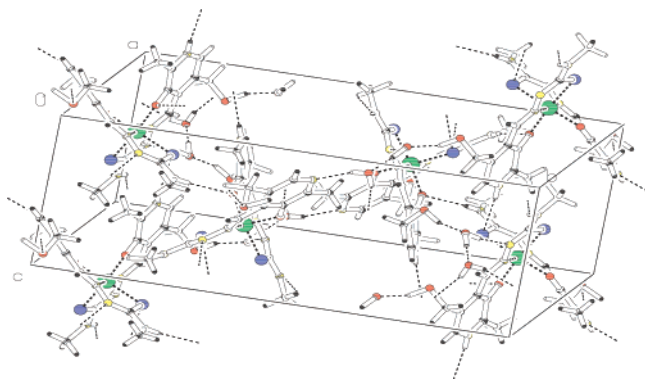


Figure 4. Packing arrangement of $[\text{Fe}(\text{Hmthpy})(\text{mthpy})]\cdot 2\text{H}_2\text{O}$ displayed in the unit cell. Hydrogen bonds are shown as single dotted lines.

Table 2. Selected Bond Lengths (Å) and Bond Angles (deg) for $[\text{Fe}(\text{Hthpy})(\text{thpy})]\cdot \text{CH}_3\text{OH}\cdot 3\text{H}_2\text{O}$ (**1**) and $[\text{Fe}(\text{Hmthpy})(\text{mthpy})]\cdot 2\text{H}_2\text{O}$ (**2**)^a

	1	2		1	2
Fe–S1	2.2508(14)	2.2453(11)	S1–Fe–S2	88.38(5)	90.97(4)
Fe–S2	2.2549(13)	2.2471(11)	S1–Fe–O1	176.83(10)	176.74(9)
Fe–O1	1.939(3)	1.904(3)	S1–Fe–O3	90.02(10)	94.40(8)
Fe–O3	1.930(3)	1.912(3)	S1–Fe–N1	84.99(11)	84.95(9)
Fe–N1	1.917(4)	1.940(4)	S1–Fe–N5	92.91(11)	88.75(9)
Fe–N5	1.916(4)	1.926(4)	S2–Fe–O1	94.46(10)	86.36(8)
S1–C9	1.726(4)	1.755(4)	S2–Fe–O3	176.64(8)	174.63(8)
S2–C18	1.738(4)		S2–Fe–N1	92.56(10)	95.66(9)
S2–C19		1.730(4)			
O1–C6	1.315(4)	1.319(4)	S2–Fe–N5	84.7(1)	86.04(9)
O3–C15	1.321(5)		O1–Fe–O3	87.22(13)	88.27(11)
O3–C16		1.303(4)			
N3–C9	1.330(5)	1.305(5)	O1–Fe–N1	93.47(13)	93.46(11)
N4–C9	1.339(6)	1.348(5)	O1–Fe–N5	88.76(13)	92.93(12)
N7–C18	1.316(5)		O3–Fe–N1	90.25(13)	84.54(11)
N8–C18	1.361(5)				
N7–C19		1.322(5)	O3–Fe–N5	92.43(12)	94.35(11)
N8–C19		1.334(5)			
N2–C4	1.341(6)	1.346(6)	N1–Fe–N5	176.60(14)	173.49(13)
N2–C5	1.345(5)	1.317(5)	C13–N6–C14	119.2(3)	
N6–C13	1.349(6)		C4–N2–C5	121.2(4)	118.4(3)
N6–C14	1.326(6)	1.347(6)	C14–N6–C15		124.3(4)
N6–C15		1.333(5)			
N1–N3	1.403(5)	1.408(4)			
N1–C1	1.299(5)	1.284(5)			
N5–N7	1.400(5)	1.380(4)			
N5–C10	1.296(5)				
N5–C11		1.302(5)			

^a Standard deviations in the last decimal place are given in parentheses.

at the cis-positions and N at the trans-positions. The singly deprotonated ligand is in its zwitterionic form, whereas the doubly deprotonated ligand does not possess any hydrogen at the pyridine nitrogen. Protonation is evident from the values of the C4–N2–C5 and C14–N6–C15 of the pyridyl angles of 121.2(4)° and of 124.4(4)° for **1** and **2**, respectively, which have significantly increased with respect to the C13–N6–C14 and C4–N2–C5 angles of 119.2(3)° and of 118.4(3)° for their corresponding nonprotonated ones. This structural difference is easily seen from the C–N bond distances about the pyridyl nitrogen, which are equal for the protonated nitrogen and meaningfully different for their nonprotonated homologues. One major motivation for this study is to characterize the structural differences between the two ligands and determine whether a change of the N-substituent on the ligand part may have some effects on the geometry of the complex.

The chemical inequivalency of the mono- and dianionic ligands is characterized by the intramolecular distances tabulated in Table 2. As expected, the C–S bond length for the singly deprotonated form is slightly shorter than that of the doubly deprotonated ligand [S1–C9 = 1.726(4) Å, S2–C18 = 1.738(4) Å for **1** and S1–C9 = 1.755(4) Å, S2–C19 = 1.730(4) Å for **2**]. In both cases, they appear to be substantially longer than those observed in the free ligand pyridoxal thiosemicarbazone [C–S = 1.70(1) Å]⁴¹ and pyridoxal 4-methylthiosemicarbazone hydrochloride [C–S = 1.669(5) Å].⁴² The longer C–S distance is therefore a consequence of the chelate of its thiol form being attached to the metal ion. This thiol form is also identified by the fact that the hydrazinic nitrogens (N3, N7) are not bonded to any hydrogen atom and have a C–N distance that is within the range found for C=N double bonds. However, the bond lengths of the hydrazinic nitrogen to carbon are equal to its adjacent C–N bond lengths for the mono-deprotonated ligand but considerably different for the di-deprotonated counterparts. The question of whether the equivalency is a result of electron delocalization within the entire thiosemicarbazone moiety and whether this difference would be related to the basicity of the two types of nitrogen atoms cannot be answered at present.

X-ray structural data of Fe(III) bis-ligand compounds of the dianion of R-salicylaldehyde thiosemicarbazone reveal that the Fe–S, Fe–O, and Fe–N distances typically are on the order of 2.44, 1.96, and 2.12 Å for high-spin Fe(III), severally, whereas these are 2.23, 1.94, and 1.96 Å for low-spin Fe(III), severally.⁴³ Comparison with these iron ligand bond lengths indicates that the Fe(III) ion is in the low-spin state in the present compounds at 100(1) K.

The major difference between these two compounds resides in the substituent at the terminal N position. Moreover, the C–N and N–N bond distances about the azomethine nitrogens (N1, N5) are also indicative. For complex **1**, these distances are equal for the two inequivalent complexing agents, which is not the case observed for complex **2**, though the difference is sufficiently small. This is related to the planarity of the ligands in the Fe(III) compounds. Thus, the octahedron formed in **1** is less distorted compared to that formed in complex **2**. This is in agreement with the N1–Fe–N5 bond angles of 176.60(14) for **1** and of 173.49(13) for **2**, respectively.

The packing of the molecules in the unit cell as viewed along the three-dimensional axes is shown in Figures 3 and 4. The molecules of both compounds are held together by N–H···O, N–H···S, O–H···S, O–H···N, and O–H···O hydrogen bonds. A summary of the hydrogen-bond dimensions is given in Table 3. The most striking ones are those formed in complex **2**, which will be described in detail.

One of the H₂O molecules, O5, forms two short O–H···O hydrogen bonds as a donor, one to O6 with an

(41) Belicchi Ferrari, M.; Fava Gasparri, G.; Leporati, E.; Pelizzi, C.; Tarasconi, P.; Tosi, G. *J. Chem. Soc., Dalton Trans.* **1986**, 2455.

(42) Abram, U.; Ortnor, K.; Gust, R.; Sommer, K. *J. Chem. Soc., Dalton Trans.* **2000**, 735.

(43) Zelensov, V. V. In *Advances in Inorganic Chemistry*, 6th ed.; Spitsyn, V. I., Ed.; MIR Publishers 1983; p 122.

Table 3. Geometry of Intra- and Intermolecular Hydrogen Bonds for [Fe(Hthpy)(thpy)]·CH₃OH·3H₂O (**1**) and [Fe(Hmthpy)(mthpy)]·2H₂O (**2**)^{a,b}

D—H···A	D—H (Å)	H···A (Å)	D···A (Å)	D—H···A (deg)
(a) For 1				
O4—H24···O5 ^b	0.84(10)	2.08(10)	2.838(5)	151(9)
N2—H25···O7 ^a	0.82(12)	2.02(12)	2.831(7)	168(12)
N4—H26···O2 ^c	0.86(6)	2.08(6)	2.918(6)	166(6)
N8—H27···O4 ^d	0.80(5)	2.29(5)	3.074(5)	167(5)
N8—H27'···O1 ^d	0.88(5)	2.33(5)	3.100(5)	146(4)
O5—H51···O6	0.86(7)	1.92(7)	2.768(6)	171(6)
O5—H51'···O4 ^e	0.86(9)	2.10(9)	2.817(5)	141(8)
O6—H61···O3	0.85(5)	2.08(5)	2.926(6)	172(6)
O6—H61'···O8B	0.86(5)	2.00(6)	2.856(11)	175(6)
O7—H71···O8A ^f	0.91(4)	2.23(8)	2.807(13)	121(7)
O7—H71'···O5	0.87(4)	2.10(5)	2.919(6)	158(5)
(b) For 2				
O2—H22···S2 ^{a'}	1.29(14)	2.33(15)	3.565(3)	159(10)
O4—H24···O5 ^{b'}	1.05(7)	1.60(7)	2.611(5)	159(6)
O5—H25···O6	1.03(6)	1.66(6)	2.689(6)	177(6)
O5—H25···N7	0.95(7)	1.88(7)	2.821(5)	168(6)
O6—H26···N3 ^{b'}	0.76(9)	2.37(10)	2.952(6)	134(9)
O6—H26···N2 ^{c'}	0.79(7)	2.00(7)	2.766(5)	165(7)
N4—H34···O3 ^{d'}	0.80(5)	2.30(4)	3.081(4)	166(4)
N6—H36···S1 ^{e'}	0.82(4)	2.49(4)	3.312(4)	175(3)
N8—H38···O2 ^{f'}	0.79(5)	2.24(5)	2.928(5)	147(4)

^a Standard deviations in the last decimal place are given in parentheses.

^b Atoms marked with a letter are generated by the following symmetry operations: a = 1 - x, 1 - y, -z; b = 1 + x, y, z; c = -x, 2 - y, -z; d = 1 - x, 2 - y, 1 - z; e = 1 - x, 1 - y, 1 - z; f = -x, 1 - y, -z; a' = -x, -y, -z; b' = x, 1/2 - y, 1/2 + z; c' = 1 - x, -y, -z; d' = x, 1/2 - y, 1/2 + z; e' = x, y, -1 + z; f' = 1 + x, y, 1 + z.

O5—O6 distance of 2.689(6) Å and another to O4 while it acts as an acceptor with the O4—O5 separation of 2.611(5) Å. The third hydrogen-bond involves N7 as an acceptor, and has a normal contact with a O5—N7 distance of 2.821(5) Å. The result is the triangular configuration adopted by this water molecule, linking to N/O atoms at all its apexes.

The second H₂O solvate molecule, O6, forms one weak and one normal O—H···N contact to the hydrazinic-N3 and pyridine-N2 nitrogen, respectively. The O6—N3 distance of 2.952(6) Å is a hydrogen bond. This O6—H26···N3 hydrogen bond together with the O6—H26'···N2 contact links the molecules in the *a* direction.

Although the O—H···S hydrogen bond is rare, our value of 3.565(3) Å for the O2—S2 distance is longer than the other reported cases,⁴⁴ the range for the hydrogen bonding being 3.21–3.37 Å. However, the H22—S2 contact of 2.33(15) Å is definitely less than the van der Waals contact of 2.6 Å. The slight shortening of the H22—S2 distance together with the satisfactory O2—H22···S2 angle of 159(10)° leads us to suggest that this contact is a very weak O—H···S hydrogen bond. The protonated nitrogen of the pyridine ring forms one weak N—H···S hydrogen bond to S1 with an N6—S1 distance of 3.312(4) Å. The result is the linking of the molecules along the *c* direction. The nitrogen at the terminal N position also forms hydrogen bonds with oxygen atoms. One CH₃NH group, N4, forms a short N—H···O contact to O3. The N4—O3 distance of 3.081(4) Å is a hydrogen bond with a satisfactory N—H···O angle of 166(4)°. The second

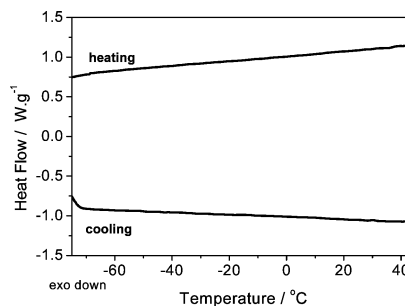


Figure 5. Low-temperature (−80 to 50 °C) part of the DSC curves comparable for both compounds.

CH₃NH group, N8, forms a normal contact of 2.928(5) Å to O2, and the result is that it links the molecules along the *ac* plane.

The result of the hydrogen bonding is a spider-web-like structure formed by O—H···O and O—H···N hydrogen bonds extending in the base vector. The spider webs are linked together by weak O—H···S, N—H···O, and N—H···S hydrogen bonds.

Magnetic and Thermal Studies. Low-Temperature Measurements. The low-temperature heat flow curves of **1** and **2** are shown in Figure 5. No thermal anomalies are found in these curves (heating and cooling, respectively), pointing out the absence of a phase transition in this temperature range. This result correlates well with the variable temperature magnetic data presented in Figure 6 recorded from 5 up to 300 K. No change of spin state is observed in both compounds during heating and cooling runs. Thus, **1** and **2** remain low-spin.

Thermogravimetric Results. The observed percentage weight loss corresponding to the first inflection in the thermograms of both compounds was compared (Figure 7) with those calculated on the basis of possible decomposition of the expelled moieties. In the present study, the TGA profile consists of two well-defined stages. On heating between 84 and 130 °C, the complexes liberate solvate molecules. The theoretical weight loss for this step is 13.89% for **1** and 6.03% for **2**. The experimental losses of weight are 13.20% and 6.29% for **1** and **2**, respectively, which are very close to the theoretical values. Here the compounds are completely devoid of lattice solvent molecules. Then the curves showed a straight line that did not change, even on heating up to 224 °C, indicating that there is no further change in weight. Finally, the last step of decomposition starts from around 224 °C and continues even beyond 250 °C, involving deterioration of the compounds.

High-Temperature Measurements. The high-temperature DSC curves, as displayed in Figure 8, were measured in agreement with the TGA results up to the same temperature. For **2**, curves show an endothermic feature accompanied with a broad shoulder in the first heating from room temperature up to 180 °C. As is reported in the literature,^{45,46} the shoulder belongs to the desorption of solvate molecules, while the spin state change occurrence corresponds to the peak. This

(44) *Conformation of Biopolymers*; Academic Press: New York, 1967; Vol. 2, p 607.

(45) Papánková, B.; Vrbová, M.; Boca, R.; Simon, P.; Falk, K.; Míche, G.; Fuess, H. *J. Therm. Anal. Calorim.* **2002**, *67*, 721.

(46) Boca, R.; Linert, W. *Monatsh. Chem.* **2003**, *134*, 199.

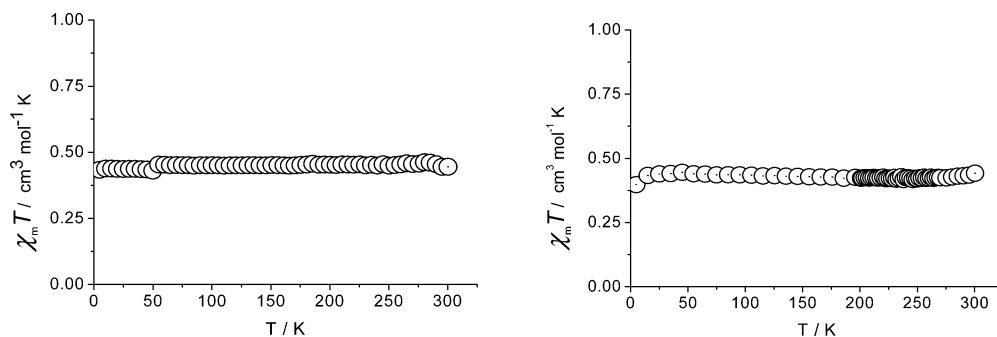


Figure 6. Temperature dependence (5–300 K) of $\chi_m T$ for $[\text{Fe}(\text{Hthpy})(\text{thpy})]\cdot\text{CH}_3\text{OH}\cdot 3\text{H}_2\text{O}$ (left) and for $[\text{Fe}(\text{Hmthpy})(\text{mthpy})]\cdot 2\text{H}_2\text{O}$ (right).

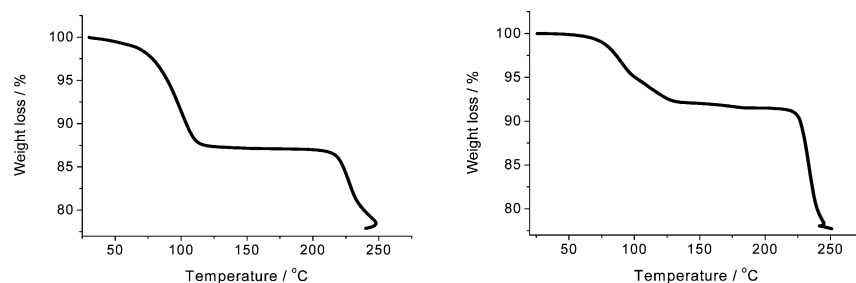


Figure 7. TGA curve of $[\text{Fe}(\text{Hthpy})(\text{thpy})]\cdot\text{CH}_3\text{OH}\cdot 3\text{H}_2\text{O}$ (left) and of $[\text{Fe}(\text{Hmthpy})(\text{mthpy})]\cdot 2\text{H}_2\text{O}$ (right).

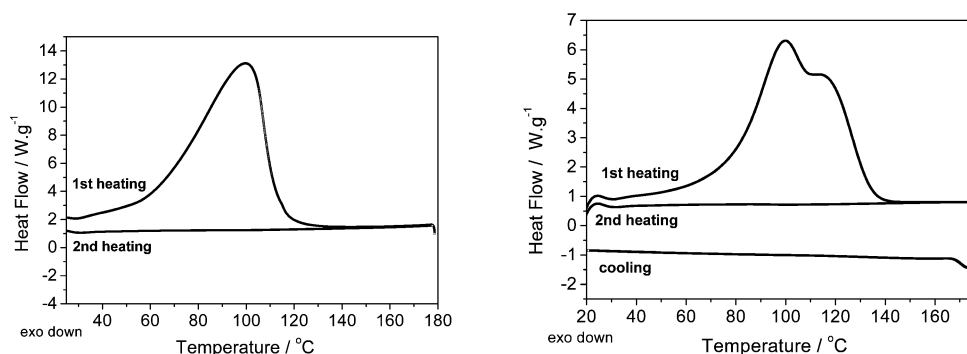


Figure 8. High-temperature (20–180 °C) part of the DSC curves of $[\text{Fe}(\text{Hthpy})(\text{thpy})]\cdot\text{CH}_3\text{OH}\cdot 3\text{H}_2\text{O}$ (left) and $[\text{Fe}(\text{Hmthpy})(\text{mthpy})]\cdot 2\text{H}_2\text{O}$ (right).

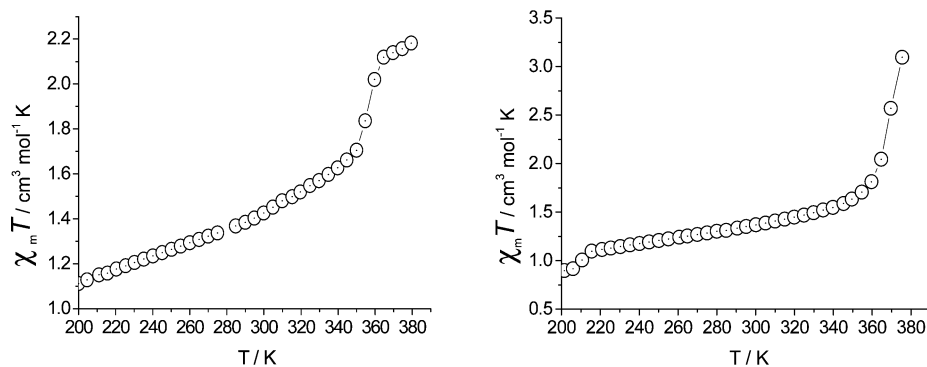


Figure 9. Temperature dependence (200–375 K) of $\chi_m T$ for $[\text{Fe}(\text{Hthpy})(\text{thpy})]\cdot\text{CH}_3\text{OH}\cdot 3\text{H}_2\text{O}$ (left) and for $[\text{Fe}(\text{Hmthpy})(\text{mthpy})]\cdot 2\text{H}_2\text{O}$ (right).

peak is totally absent in the second heating curve when it was measured immediately after cooling down to room temperature, without allowing the compounds (to stand for) a possible rehydration, since the rehydration process was not possible under these experimental conditions. Similar behavior is observed for **1**; however, the curve shows no discontinuity and is rounded at the top. Thus, we suggested that, after switching to a new phase, the compounds do not undergo any further phase transition. This result is supported on one hand by the high-temperature (200–380 K) magnetic

behavior of **1** and **2**, displayed in Figure 9. Evidently, the product of the magnetic susceptibility and the temperature ($\chi_m T$) of **1** and **2** exhibits significant temperature dependence. In both cases, the compounds remain in their low-spin state up till 350 K for **1** and 360 K for **2**, before changing abruptly to the high-spin state. Because Mössbauer spectroscopy shows the spin state, liberation of solvent molecules thus accompanies the interconversion of Fe(III) spin states, which has further been monitored by ^{57}Fe Mössbauer spectroscopy and is to be published elsewhere. On the other hand, the

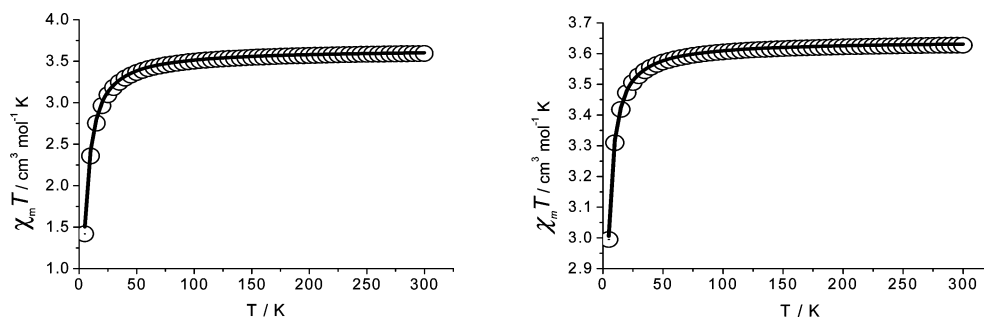


Figure 10. Temperature dependence (5–300 K) of $\chi_m T$ for $[\text{Fe}(\text{Hthpy})(\text{thpy})]\cdot\text{CH}_3\text{OH}\cdot 3\text{H}_2\text{O}$ (left) and for $[\text{Fe}(\text{Hmthpy})(\text{mthpy})]\cdot 2\text{H}_2\text{O}$ (right), after placing in an oven at 453 K for about 2 h. The solid line corresponds to the fit using the parameters described in the text.

$\chi_m T$ vs T plots for the nonsolvated compounds as viewed in Figure 10 are more pronounced. After treating samples in an oven at 453 K for about 2 h, the value of $\chi_m T$ varies from $3.59 \text{ cm}^3 \text{ mol}^{-1} \text{ K}$ at 300 K to $1.42 \text{ cm}^3 \text{ mol}^{-1} \text{ K}$ at 5 K for **1** and from $3.63 \text{ cm}^3 \text{ mol}^{-1} \text{ K}$ at 300 K to $2.99 \text{ cm}^3 \text{ mol}^{-1} \text{ K}$ at 5 K for **2**. The product of the magnetic susceptibility and the temperature clearly shows a plateau equal to $3.59 \text{ cm}^3 \text{ mol}^{-1} \text{ K}$ for **1** and to $3.63 \text{ cm}^3 \text{ mol}^{-1} \text{ K}$ for **2**, between 50 and 300 K, which is close to the expected value of $3.9 \text{ cm}^3 \text{ mol}^{-1} \text{ K}$ for a sextuplet high-spin state ($S = 5/2$). Below 20 K, $\chi_m T$ drops rather abruptly, reflecting the large zero-field splitting (ZFS) of the ground state, which is usual in high-spin Fe(III) porphyrins.^{47,48} The data were fitted using the following equation:

$$\chi_m = \frac{Ng^2\beta^2}{4kT} \left[\frac{0.14 + 5.12e^{-3.23X} + 23.85e^{-6.83X}}{1 + e^{-3.23X} + e^{-6.83X}} \right] \quad (5)$$

Where, $X = D/kT$, D is the zero-field splitting parameter, g is the Landé factor, and the other symbols have their usual meanings. Equation 5 is the theoretical equation for the magnetic susceptibility resulting from the axial and rhombic zero-field splitting for an $S = 5/2$ ion.⁴⁹ The best fit has been obtained with the parameters $D = 0.899(9) \text{ cm}^{-1}$ and $g = 2.002(9)$ with a coefficient of determination (COD) of $R^2 = 0.996$ and a reduced χ^2 of 0.0005 for **1** and $D = 0.223(1) \text{ cm}^{-1}$ and $g = 2.0009(2)$ with a COD of $R^2 = 0.997$ and a reduced χ^2 of 0.00002 for **2**. Reduced χ^2 measures the appropriateness of the fits and it is obtained from the following function:

$$\chi^2 = \left[\frac{\sum (\chi_{\text{obs}} T - \chi_{\text{calc}} T)^2}{\sum \chi_{\text{obs}} T} \right] \quad (6)$$

where $\chi_{\text{obs}} T$ and $\chi_{\text{calc}} T$ are the observed and calculated product of the magnetic susceptibility and the temperature respectively.

Heat Capacity, Enthalpy, and Entropy. The heat capacity is a thermodynamically well-defined quantity and opens the way to determine thermodynamically potential functions.²² In order to calculate the enthalpy and entropy changes

Table 4. Molar Experimental Heat Capacities of the LS Phase for $[\text{Fe}(\text{Hthpy})(\text{thpy})]\cdot\text{CH}_3\text{OH}\cdot 3\text{H}_2\text{O}$ (**1**) and $[\text{Fe}(\text{Hmthpy})(\text{mthpy})]\cdot 2\text{H}_2\text{O}$ (**2**)

T (K)	C_p ($\text{J mol}^{-1} \text{ K}^{-1}$)		T (K)	C_p ($\text{J mol}^{-1} \text{ K}^{-1}$)	
	1	2		1	2
232.95	738.400	630.912	278.04	783.178	699.176
238.00	739.598	639.296	283.04	792.872	705.831
242.94	741.701	647.300	288.01	803.442	712.266
248.00	744.811	655.347	293.03	815.066	718.582
252.96	748.798	663.038	298.06	827.668	724.727
258.00	753.800	670.669	303.02	841.029	730.605
262.95	759.646	677.983	308.03	855.468	736.360
268.00	766.564	685.260	312.94	870.539	741.823
273.05	774.445	692.351			

Table 5. Molar Experimental Heat Capacities of the HS Phase for $[\text{Fe}(\text{Hthpy})(\text{thpy})]\cdot\text{CH}_3\text{OH}\cdot 3\text{H}_2\text{O}$ (**1**) and $[\text{Fe}(\text{Hmthpy})(\text{mthpy})]\cdot 2\text{H}_2\text{O}$ (**2**)

T (K)	C_p ($\text{J mol}^{-1} \text{ K}^{-1}$)		T (K)	C_p ($\text{J mol}^{-1} \text{ K}^{-1}$)	
	1	2		1	2
403.07	754.142		453.07	938.063	1087.326
408.01	770.266		458.77	961.949	1112.772
413.03	787.112	924.828	463.13	980.623	1132.625
418.33	805.400	944.704	468.23	1002.910	1156.276
422.68	820.796	961.390	472.97	1024.053	1178.671
427.98	840.025	982.173	478.04	1047.125	1203.066
432.97	858.601	1002.196	483.02	1070.247	1227.473
437.96	877.635	1022.662	488.00	1093.826	1252.319
442.95	897.126	1043.569	493.06	1118.250	1278.016
447.94	917.076	1064.918			

connected with the spin transition of both complexes, the magnetic contribution to the heat capacity was evaluated by subtracting from the experimentally measured quantities the contributions arising from the lattice vibrations.⁵⁰ A comparison of the experimental heat capacities of the LS and HS phase in the vicinity of the peak for $[\text{Fe}(\text{Hthpy})(\text{thpy})]\cdot\text{CH}_3\text{OH}\cdot 3\text{H}_2\text{O}$ (**1**) and $[\text{Fe}(\text{Hmthpy})(\text{mthpy})]\cdot 2\text{H}_2\text{O}$ (**2**) are given in Tables 4 and 5. It is evident from an examination of these tables that there are lattice contributions to the heat capacity of both compounds, otherwise one would expect to have the same values of heat capacity in LS phase of **1** and **2** as well as in the HS phase, respectively. In Table 1 are listed the formula weights, the lattice constants a , b and c , the axial ratio c/a , and the volume per unit cell ($Z = 2$ for **1** and $Z = 4$ for **2**) of the compounds. The variation in structural parameters is not large, although evidently it is great enough so that thermal properties of the lattice are not identical for both complexes. Another observation from Tables 4 and 5 is the values of the heat capacity of compound **1** in the HS state. At the beginning of this phase, the heat

(47) Mitra, S. In *Iron Porphyrins*; Lever, A. B. P., Gray, H., Eds.; Addison-Wesley: Reading, MA, 1983; Part II, p 1.

(48) Mazzanti, M.; Marchon, J. C.; Wojaczyski, J.; Wolowicz, S.; Granzynski, L. L.; Shang, M.; Scheidt, W. R. *Inorg. Chem.* **1998**, *37*, 2476.

(49) Chen, C.-H.; Lee, Y.-Y.; Liao, B.-C.; Elango, S.; Chen, J.-H.; Hsieh, H.-Y.; Liao, F.-L.; Wang, S.-L.; Hwang, L.-P. *J. Chem. Soc., Dalton Trans.* **2002**, 3001.

(50) Stout, J. W.; Catalano, E. *J. Chem. Phys.* **1955**, *23*, 2013.

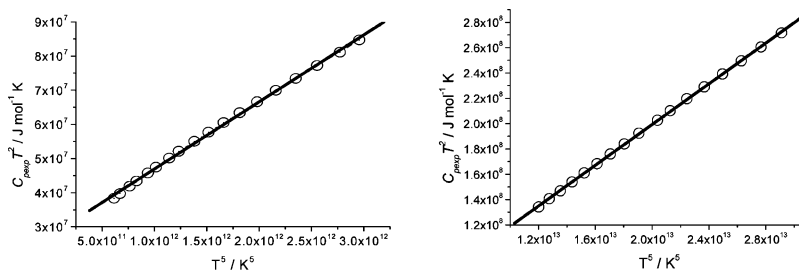


Figure 11. LS (left) and HS (right) phase graphs ($C_{p,\text{exp}} T^2$ vs T^5) showing the comparability of the procedure used for both compounds. The solid straight lines correspond to the fit using the parameters described in the text.

capacity data are even smaller compared to those of the LS phase in the immediate vicinity of the transition peak. By extrapolating, one can affirm that the values have achieved a maximum and then dropped to a minimum before starting to increase with increasing temperature in the HS phase. Similar behavior has already been reported in the literature,^{51–56} and it was proven from ⁵⁷Fe Mössbauer spectroscopy analysis that this drop in heat capacity values in the HS state shows the presence of the LS fraction in the phase and it disappears just at the temperature where the values of the heat capacity become larger.⁵⁶ In Figure 11 are presented the plots ($C_{p,\text{exp}} T^2$ vs T^5) showing the applicability of the procedure used; a and b constants were determined with the best fit to the data and resulted in $a_{\text{LS}} = (1.96 \pm 0.02) \times 10^{-5}$, $b_{\text{LS}} = (2.73 \pm 0.03) \times 10^7$ for the LS phase measurements and $a_{\text{HS}} = (8.04 \pm 0.02) \times 10^{-6}$, $b_{\text{HS}} = (3.85 \pm 0.05) \times 10^7$ for the HS phase measurements, both for complex **1**, and $a_{\text{LS}} = (1.69 \pm 0.05) \times 10^{-5}$, $b_{\text{LS}} = (2.45 \pm 0.08) \times 10^7$ for the LS phase measurements and $a_{\text{HS}} = (8.93 \pm 0.04) \times 10^{-6}$, $b_{\text{HS}} = (5.18 \pm 0.08) \times 10^7$ for the HS phase measurements, both for compound **2**.

The differences between measured heat capacities and estimated lattice heat capacities were numerically integrated with respect to the initial (T_i) and the final temperature (T_f) for LS and HS phase, respectively, within the measured temperature region. The excess enthalpy and entropy related to the spin state changes are $\Delta H = (12.5 \pm 0.3) \text{ kJ mol}^{-1}$, $\Delta S = (33.3 \pm 0.8) \text{ J mol}^{-1} \text{ K}^{-1}$ for complex **1** and $\Delta H = (6.5 \pm 0.3) \text{ kJ mol}^{-1}$, $\Delta S = (17.6 \pm 0.8) \text{ J mol}^{-1} \text{ K}^{-1}$ for complex **2**. For compound **1**, the entropy gain is close to the range forecasted,^{57–59} while its excess enthalpy is even larger than the theoretical predicted value.⁵⁹ Though this entropy is acceptable, it seems large enough compared to those published on ferric thiosemicarbazones complexes,^{40,60}

since it is clear from the X-ray study that methanol solvate is disordered in the crystal lattice; consequently, one cannot exclude the possibility that the surplus enthalpy and entropy gain include the contribution from the disordering of the methanol solvate molecule. Different from **1**, compound **2** has an enthalpy gain within the range ($5\text{--}8 \text{ kJ mol}^{-1}$) observed for the spin transition of Schiff-base ferric complexes,^{40,57–59} though its excess entropy remains smaller, it seems reasonable because the transition is taking place at high temperature ($T_c > 300 \text{ K}$) compared to many other spin crossover compounds which have their transition temperature below room temperature. Moreover, it has already been found that at the transition temperature $\Delta S = \Delta H/T_c$.⁶¹ Thus, above room temperature, if an enthalpy gain varies within the range $5\text{--}8 \text{ kJ mol}^{-1}$, then its excess entropy will not stay within this limit ($34\text{--}41 \text{ J mol}^{-1} \text{ K}^{-1}$), and the reciprocal holds true.

Comments and Conclusions. Since the very first studies, the crucial influence of crystal solvent molecules on the spin crossover behavior has been recognized. In spite of this fact, there are very few systematic investigations devoted to this issue. Compounds under study are typical examples that show the effect of solvent molecules on the spin state change occurrence. The presence of those in the crystal lattice stabilizes the low-spin state up till room temperature before an abrupt change of spin state takes place when solvate molecules are released as long as the temperature is increased. In fact, this loss of solvent molecules causes an irreversible spin state transformation. A similar observation has already been reported in the literature.^{62,63} The temperature interval where this transformation occurs corresponds rightly to that where the solvated species changes to the non-solvated ones. Hydrogen bonding also seems to play a significant role in changes in SCO behavior accompanying desolvation process. Solvated species result in a stabilization

- (51) (a) Nakamoto, T.; Bhattacharjee, A.; Sorai, M. *Bull. Chem. Soc. Jpn.* **2004**, *77*, 921. (b) Sorai, M. *Bull. Chem. Soc. Jpn.* **2001**, *74*, 2223.
 (52) Mocala, K.; Navrotsky, A.; Sherman, D. M. *Phys. Chem. Miner.* **1992**, *19*, 88.
 (53) Sorai, M.; Seki, S. *J. Phys. Soc. Jpn.* **1972**, *32*, 382.
 (54) Sorai, M.; Seki, S. *J. Phys. Chem. Solids* **1974**, *35*, 555.
 (55) Boo, W. O. J.; Stout, J. W. *J. Chem. Phys.* **1976**, *65*, 3929.
 (56) Nakamoto, T.; Tan, Z.-C.; Sorai, M. *Inorg. Chem.* **2001**, *40*, 3805.
 (57) (a) Conti, A. J.; Chadha, R. K.; Sena, K. M.; Rheingold, A. L.; Hendrickson, D. N. *Inorg. Chem.* **1993**, *32*, 2670. (b) Conti, A. J.; Kaji, K.; Nagano, Y.; Sena, K. M.; Yumoto, Y.; Chadha, R. K.; Rheingold, A. L.; Sorai, M.; Hendrickson, D. N. *Inorg. Chem.* **1993**, *32*, 2681.
 (58) Sorai, M.; Maeda, Y.; Oshio, H. *J. Phys. Chem. Solids* **1990**, *51*, 941.
 (59) Sorai, M. *Top. Curr. Chem.* **2004**, *235*, 153.
 (60) Shipilov, V. I.; Zelentsov, V. V.; Zhdanov, V. M.; Turdakin, V. A. *JETP Lett. (Engl. Transl.)* **1974**, *19*, 294.

- (61) Cantin, C.; Kliava, J.; Marbeuf, A.; Mikailitchenko, D. *Eur. Phys. J.* **1999**, *B12*, 525.
 (62) (a) Zhang, W.; Zhao, F.; Liu, T.; Yuan, M.; Wang, Z.-M.; Gao, S. *Inorg. Chem.* **2007**, *46*, 2541. (b) Codjovi, E.; Sommier, L.; Kahn, O.; Jay, C. *New J. Chem.* **1996**, *20*, 503. (c) Garcia, Y.; van Koningsbruggen, P. J.; Codjovi, E.; Lapouyade, R.; Kahn, O.; Rabardel, L. *J. Mater. Chem.* **1997**, *7*, 857. (d) van Koningsbruggen, P. J.; Garcia, Y.; Codjovi, E.; Lapouyade, R.; Kahn, O.; Fournes, L.; Rabardel, L. *J. Mater. Chem.* **1997**, *7*, 2069. (e) Garcia, Y.; van Koningsbruggen, P. J.; Lapouyade, R.; Fournes, L.; Rabardel, L.; Kahn, O.; Ksenofontov, V.; Levchenko, G.; Gütllich, P. *Chem. Mater.* **1998**, *10*, 2426. (f) Hayami, S.; Gu, Z.-Z.; Yoshiki, H.; Fujishima, A.; Sato, O. *J. Am. Chem. Soc.* **2001**, *123*, 11644. (g) Roubeau, O.; Haasnoot, J. G.; Codjovi, E.; Varret, F.; Reedijk, J. *Chem. Mater.* **2002**, *14*, 2559.
 (63) Fukukai, T.; Yabe, K.; Ogawa, Y.; Matsumoto, N.; Mrozinski, J. *Bull. Chem. Soc. Jpn.* **2005**, *78*, 1484.

Neutral Fe(III) Complexes of Thiosemicarbazones

of the LS state, through hydrogen bonding of solvent molecules with the ligand. Since the ferric thiosemicarbazone are unique among ferric spin crossover solids in that they possess an abundance of potential sites for intermolecular hydrogen-bonding interactions, the loss of these solvent molecules results in the destruction of such an interaction and completely modifies the relatively strong stability of the monomeric units in the solid state.

In conclusion, we have succeeded in synthesizing two new neutral ferric complexes of pyridoxal thiosemicarbazone and pyridoxal methylthiosemicarbazone, respectively solvated, and in characterizing the structural differences between the two ligands (Hthpy, Hmthpy and thpy, mthpy). We have also demonstrated that thermal spin-state transformation is trig-

gered by the desolvation process as well as by the destruction of the intermolecular hydrogen-bonding networks. However, for the present complexes the ΔH and ΔS values are as large as those published on the spin transition of Schiff-base ferric complexes;^{40,57–60} this fact means that the change of spin state induced by the desolvation phenomenon also involves enthalpy and entropy changes comparable with those of the cooperative spin crossover phenomenon.

Supporting Information Available: X-ray crystallographic data in CIF format. This material is available free of charge via the Internet at <http://pubs.acs.org>.

IC701695B